Talanta 85 (2011) 943–949

Contents lists available at ScienceDirect

Talanta

journal homepage: www.elsevier.com/locate/talanta

Low-temperature growth of ZnO nanoparticles: Photocatalyst and acetone sensor

Sher Bahadar Khan, M. Faisal*, Mohammed M. Rahman, Aslam Jamal

Centre for Advanced Materials and Nano-Engineering (CAMNE), Department of Chemistry, Faculty of Sciences and Arts, Najran University, P.O. Box 1988, Najran 11001, Saudi Arabia

ARTICLE INFO

Article history:
Received 22 March 2011
Received in revised form 30 April 2011
Accepted 3 May 2011
Available online 10 May 2011

Keywords:
ZnO nanoparticles
Structural properties
Optical properties
Photocatalyst
Acetone sensor

ABSTRACT

Well-crystalline ZnO nanoparticles (NPs) were synthesized in large-quantity via simple hydrothermal process using the aqueous mixtures of zinc chloride and ammonium hydroxide. The detailed structural properties were examined using X-ray diffraction pattern (XRD) and field emission scanning electron microscope (FESEM) which revealed that the synthesized NPs are well-crystalline and possessing wurtzite hexagonal phase. The NPs are almost spherical shape with the average diameters of ~50 ± 10 nm. The quality and composition of the synthesized NPs were obtained using Fourier transform infrared (FTIR) and electron dispersed spectroscopy (EDS) which confirmed that the obtained NPs are pure ZnO and made with almost 1:1 stoichiometry of zinc and oxygen, respectively. The optical properties of ZnO NPs were investigated by UV–vis absorption spectroscopy. Synthesized ZnO NPs were extensively applied as a photocatalyst for the degradation of acridine orange (AO) and as a chemi-sensor for the electrochemical sensing of acetone in liquid phase. Almost complete degradation of AO has taken place after 80 min of irradiation time. The fabricated acetone sensor based on ZnO NPs exhibits good sensitivity (~0.14065 μA cm^{-2} mM^{-1}) with lower detection limit (0.068 ± 0.01 mM) in short response time (10 s).

1. Introduction

Semiconductor nanomaterial, zinc oxide (ZnO) with its wide band-gap (~3.37 eV) is a significant functional material applicable in various fields, such as solar cells, catalysis, optical, electrical, electromagnetic shielding, biosensors, chemical and gas sensors [1]. Nano-sized semiconductor (ZnO) has received much attention due to efficient synthesis, easy to handle, cost-effectiveness, reliability and their applications as a chemi-sensor and photocatalyst for the detection of toxic chemicals such as H_2, NH_3, liquid petroleum gas (LPG), HCHO, ammonium hydroxide, and alcohols [2–4] and for the degradation of organic pollutants such as dyes and phenol, respectively.

Toxic organic compounds in the ecosystem are the main anxiety for the scientific community and regulation authorities. These monitoring agencies have close look on volatile organic compounds and also tighten the norms all over the world. Acetone, the most commonly used solvent in chemical industries and laboratories is highly volatile and hazardous to human health and living organisms. Exposure to air having high concentration of acetone vapor may cause headache, allergy, fatigue and even narcosis [5]. In case of diabetes mellitus patients, acetone sensing is very important to investigate sugar level [6]. Hence early detection and quantification of acetone in the environment is necessary and important for our safety. Recently, metal oxides have been exploited as artificial mediators for the development of reliable and efficient chemical sensors [7]. That is why low dimensional metal oxide NPs have been proposed as a redox mediator for the detection and quantification of acetone. Here our main effort is to determine minimum concentration of acetone using low dimensional ZnO NPs by simple and reliable *I–V* technique in short response time [7–12].

Similarly, toxic and hazardous organic dyes are also serious organic pollutants which create water pollution and severely contaminate the environment [13–19]. The waste water containing the organic dyes (organic pollutants) inhibits sunlight penetration which cause esthetic pollution, eutrophication and perturbations in aquatic life and also reduce photosynthetic reaction [13–15]. Therefore, due to the serious impact of dyes and other organic pollutant on the environment has provided impetus for sustained fundamental and applied research interest in the field of dye and organic pollutant removal for environmental remediation [13–16]. Many traditional techniques have been used so far for the treatment of dye waste effluents but they lost their importance due to usually non-destructive nature towards organic dye molecules, inefficient, costly, and just transfer pollutions from one phase to another, i.e. from water to another phase [16–21]. It is found that using semiconductor materials, the organic dye pollutants can be completely degraded with the help of solar or artificial lights [13–23]. Among various semiconductor materials, the photocatalytic degradation properties of titanium oxide (TiO_2) are widely investigated.

* Corresponding author. Tel.: +966 501577579.
E-mail address: mdfaisalahsan@gmail.com (M. Faisal).

0039-9140/$ – see front matter © 2011 Elsevier B.V. All rights reserved.
doi:10.1016/j.talanta.2011.05.003

However, ZnO has recently been receiving much attention due to its low-price, very simple synthesis process, bio-compatibility nature, high-stability, high-activity towards photo-induced redox reactions, various applications in photonics and electronics, photocatalytic reduction, the eradication of environmental pollutants and environmentally friendly photo-catalyst, etc. [22,23]. It is predicted that ZnO could be one of the best photo-catalysts for the degradation of organic dyes.

The aim of present study was to investigate the synthesis of low dimensional ZnO NPs via simple hydrothermal process at low-temperature and to utilize as a chemi-sensor and photocatalyst for the detection and degradation of organic pollutants. Morphological, structural and optical properties of the prepared ZnO photocatalyst were characterized by XRD, FESEM, FTIR, Raman, and UV/vis spectroscopy. Photocatalytic activity of the prepared ZnO NPs was evaluated by photodegradation of AO. Synthesized ZnO NPs were utilized to fabricate efficient chemical sensor and their performance was tested on acetone at room temperature. To the best of our knowledge, this is the first report for detection of acetone (liquid phase) using simple and reliable *I–V* technique in short response time.

2. Experimental details

2.1. Growth and characterizations

All the chemicals were of reagent grade, purchased from Aldrich and used as received. ZnO NPs were synthesized by simple hydrothermal method using the aqueous (DI water) mixtures of zinc chloride and ammonium hydroxide as source materials. In a typical reaction process, ammonium hydroxide solution was added dropwise in 0.1 M zinc chloride solution made in 100.0 mL of DI water under constant stirring. The addition of ammonium hydroxide was stopped when the pH of the solution reached 10.2. The reaction mixture was then continuously stirred for 1 more hour and the resultant solution was then transferred into a Teflon-lined autoclave and heated up to 150.0 °C for 3 h. After terminating the reaction, the autoclave was allowed to cool at room-temperature and finally white precipitates were obtained which were washed with methanol several times and dried at room-temperature. The dried products were then calcined at 400.0 °C for 3 h and characterized in detail in terms of their structural, optical, photocatalytic and sensing properties.

Structural characterizations of the synthesized product were performed using field emission scanning electron microscope (FESEM; JSM-7600F, Japan) and X-ray diffraction (XRD; X'Pert Explorer, PANalytical diffractometer) data was measured with Cu-Kα_1 radiation. Fourier transform infrared spectrometer (FT-IR; Perkin Elmer) spectrum was recorded in KBr dispersion in the range of 400–4000 cm^{-1}. UV–vis spectrum was recorded in the range of 300–800 nm (Perkin Elmer-Lambda 950, UV-visible spectrometer). Raman-scattering spectrum was measured at room-temperature with the Ar^+ laser line (λ; 513.4 nm) as an excitation source.

2.2. Photocatalytic experiments

Photocatalytic decomposition of AO was examined by optical absorption spectroscopy. The photocatalytic reaction was carried in a 250 mL beaker containing 150 mL of AO dye solution (0.03 mM) and 150 mg of ZnO NPs. Prior to irradiation, the solution was stirred in dark with continuous oxygen purging for at least 15 min in order to establish adsorption/desorption equilibrium between AO molecules and the surface of the photocatalyst. The suspension was continuously purged with oxygen bubbling throughout the experiment. Irradiation was carried out using 250 W high pressure mercury lamp. Samples (5.0 mL) were collected before and at regular intervals during the irradiation and AO solutions were separated from the photo-catalyst by centrifugation before analysis. The degradation was monitored by measuring the absorbance using UV–vis spectrophotometer (Lambda 950). The absorbance of AO (0.03 mM) was followed at 491 nm wavelength.

2.3. Fabrication of glassy carbon electrode using ZnO

Glassy carbon electrode (surface area, 0.0316 cm^2) was coated with prepared ZnO using butyl carbitol acetate (BCA) and ethyl acetate (EA) as a coating agent. Then it was kept in the oven at 60 °C for 3 h until the film got completely dry (thickness of film ~0.1 mm). Phosphate buffer solution (0.1 M at pH 7.0) was prepared by mixing 0.2 M Na_2HPO_4 and 0.2 M NaH_2PO_4 solution in 100.0 mL de-ionized water.

2.4. Detection of acetone using I–V technique

A cell was constructed consisting of NPs coated glassy carbon electrode as a working electrode and Pd wire was used as counter electrode. Acetone solution was diluted at different concentrations in DI water and used as a target chemical. Amount of 0.1 M phosphate buffer solution was kept constant as 20.0 mL for all measurement. Solution was prepared with various concentrations (0.13 mM to 1.33 M) of acetone in DI water. The ratio of voltage and current (slope of calibration curve) was used as a measure of acetone sensitivity. Electrometer was used as a voltage sources for *I–V* measurement in simple two electrode system.

3. Results and discussion

3.1. Structural and optical properties of synthesized ZnO nanoparticles

General structural characterization of the synthesized products was done using FESEM and demonstrated in Fig. 1. It is clear from the FESEM images that the synthesized products are NPs which are grown in a very high-density and possessing almost uniform shape and sizes (Fig. 1(a) and (b)). Fig. 1(c) exhibits the high-resolution FESEM image of the synthesized NPs which revealed that most of the NPs possessing spherical shapes while some elongated NPs were also seen in the micrograph. The average sizes of the grown NPs were in the range of $\sim 50 \pm 10$ nm. To check the composition of the synthesized NPs, FESEM–EDS studies were done and shown in Fig. 1(d). It is clear from the EDS analysis that the synthesized NPs are composed of zinc and oxygen, only. No other peak related with any impurity has been detected in the FESEM–EDS, until the detection limit of EDS, which confirms that the synthesized NPs are made only with zinc and oxygen.

To check the crystallinity and crystal structures of the synthesized NPs, X-ray diffraction was done and result is shown in Fig. 2. It is observed from the obtained pattern that all of the indexed peaks are well-matched with that of bulk wurtzite hexagonal well-crystalline ZnO (JCPDF # 089-0511) which confirms that the synthesized NPs are well-crystalline ZnO. All the obtained peaks in the pattern belong only to ZnO and no other peak related to impurities was detected within the detection limit of the X-ray diffraction, further confirms that the obtained NPs are pure ZnO with wurtzite hexagonal phase.

The optical property of the synthesized ZnO NPs was examined using UV–vis spectrophotometer at room-temperature and shown in Fig. 3(a). To measure the UV–vis absorption, the ZnO NPs were dispersed in distilled DI water and measured. The obtained UV absorption exhibits a well-defined exciton band at 375 nm, a characteristic and corresponding peak to the wurtzite hexagonal

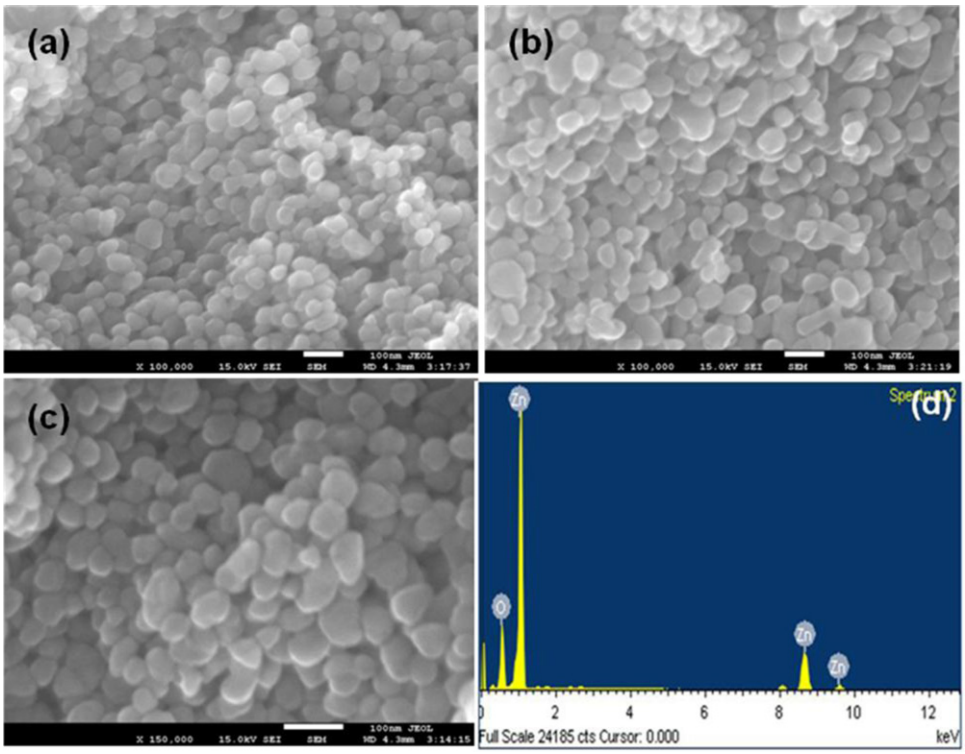

Fig. 1. Typical (a) and (b) low-magnification and (c) high-resolution FESEM images and (d) EDS spectrum of synthesized ZnO NPs.

phase bulk ZnO [24–26]. No other peak related with impurities and structural defects were observed in the spectrum which confirms that the synthesized NPs were crystalline and pure ZnO. The band gap energy was found to be 3.3 eV calculated on the basis of the maximum absorption band of ZnO NPs using Eq. (A):

$$E_{bg} = \frac{1240}{\lambda}\,(\text{eV}) \qquad \text{(A)}$$

where E_{bg} is the band-gap energy and λ is the wavelength (nm) of the ZnO NPs.

To further check the composition and quality of the synthesized ZnO NPs, FTIR studies were done in the range of 430–4000 cm^{-1} and results are shown in Fig. 3(b). Appearance of a sharp and strong band at 499 cm^{-1} in the FTIR spectrum is due to the formation of Zn–O bonds in the synthesized product. In addition to this, two other bands appeared at ~3447 cm^{-1} and ~1622 cm^{-1} indicate the presence of O–H stretching and bending modes of vibrations,

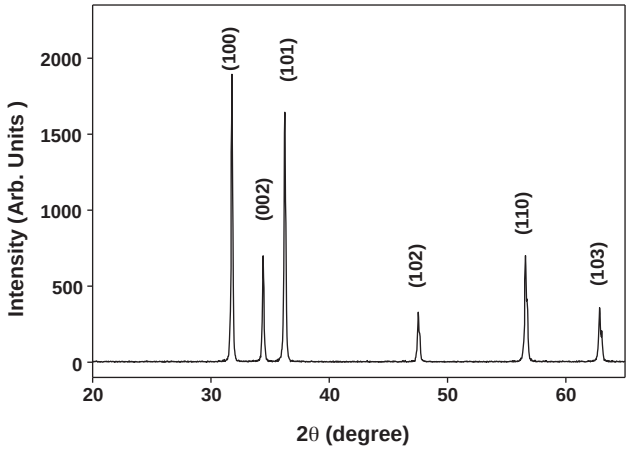

Fig. 2. Typical XRD pattern of synthesized ZnO NPs.

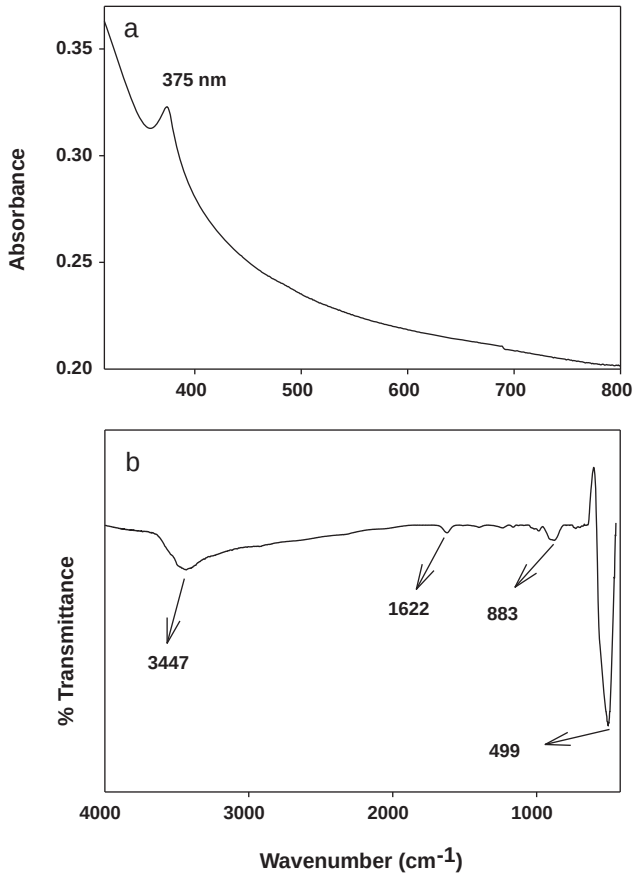

Fig. 3. Typical (a) UV–vis spectrum and (b) FTIR spectrum of synthesized ZnO NPs.

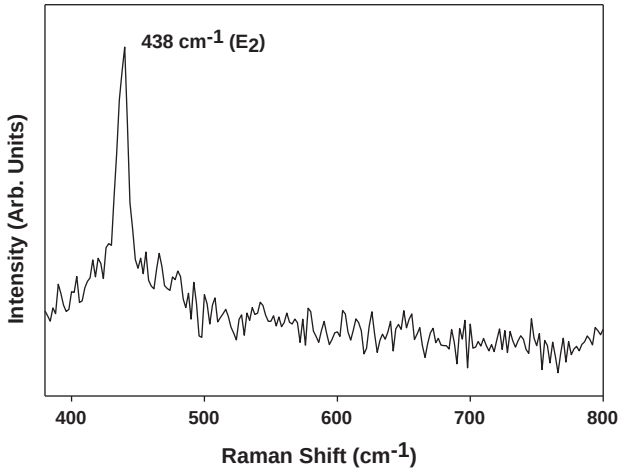

Fig. 4. Typical Raman scattering spectrum of the synthesized ZnO NPs.

respectively in the synthesized NPs. A very small band originated at 883 cm^{-1} is probably due to the carbonate moieties which generally observed when FTIR samples are measured in air [25–27].

The Raman-scattering studies are sensitive towards the crystallization, structural disorders and defects in nanostructures. Therefore, Raman-scattering studies have been performed for the synthesized ZnO NPs and shown in Fig. 4. With a wurtzite crystal structure, ZnO belongs to the C^4_{6v} space group and possess two formula units per primitive cell where all the atoms are occupying the C_3V symmetry. The group theory predicts the existence of different optic modes near the centre of the Brillouin zone which are denoted as: $\Gamma = A_1 + 2B_1 + E_1 + 2E_2$ where A_1, E_1, and $2E_2$ modes are Raman active while A_1 and E_1 are infrared active and splits into longitudinal (LO) and transverse (TO) optical components [28,29]. In case of synthesized ZnO NPs, the obtained Raman-scattering spectrum exhibits a strong and sharp peak at 438 cm^{-1}, corresponds to the optical phonon $E_{2(high)}$ mode of wurtzite hexagonal phase pure ZnO [29]. Therefore, due to the presence of only sharp and strong E_2 mode in the obtained Raman-scattering spectrum, it indicates that the synthesized ZnO NPs possess good crystal quality with the wurtzite hexagonal phase.

4. Applications

4.1. Photocatalytic degradation

Fig. 5(a) exhibits change in absorption spectra of AO as a function of irradiation time in the presence of ZnO NPs. It has been observed that irradiation of aqueous suspension of AO in the presence of ZnO NPs leads to the decrease in absorption intensity. It can be seen that the maximum absorbance at 491 nm gradually decreases with increase in irradiation time and disappear almost completely after 80 min which indicates that the AO dye has almost completely degraded after 80 min.

Irradiation of an aqueous solution of AO in the presence of synthesized ZnO NPs and commercially available TiO_2-UV100 leads to decrease in absorption intensity. Fig. 5(b) shows the change in absorbance as a function of irradiation time for the dye derivative in the absence and presence of ZnO NPs and TiO_2-UV100.

Fig. 5(c) shows a plot for the % degradation vs. irradiation time (min) for the oxygen saturated aqueous suspension of AO in the presence and absence of different photocatalysts. It could be seen from the figure that 86.36% (in the presence of TiO_2-UV100) and 96.11% (in the presence of ZnO NPs) of the compounds were

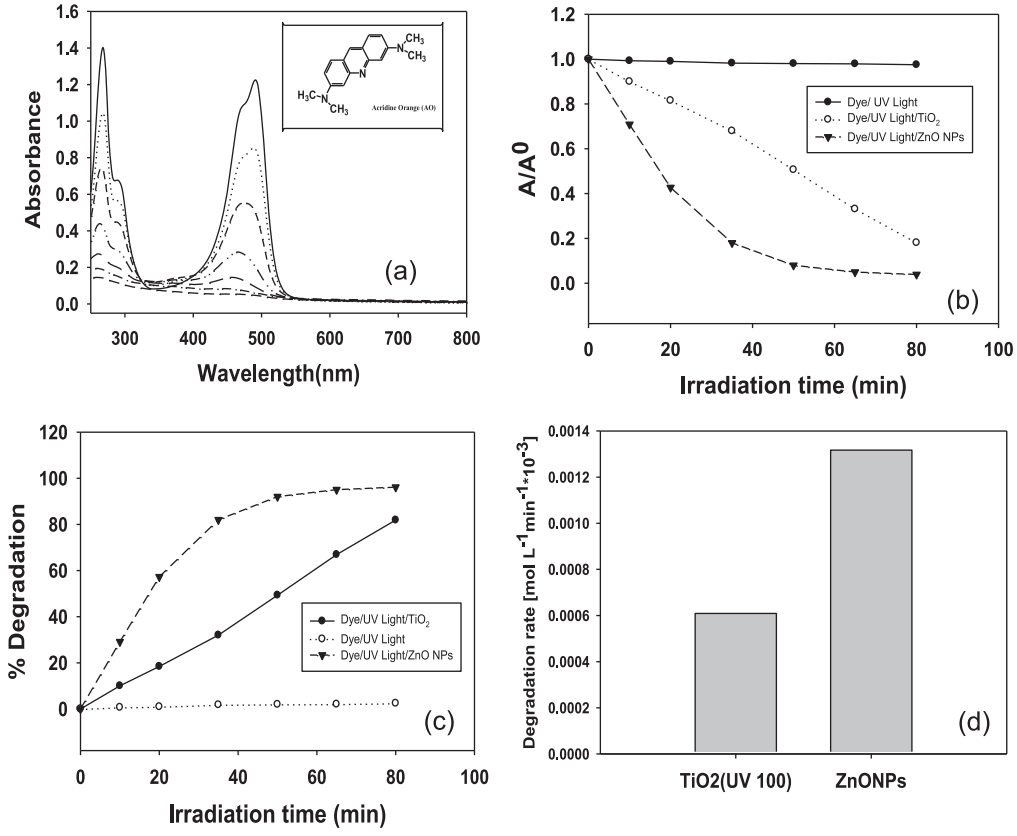

Fig. 5. Typical plot for (a) change in the absorption spectrum at different time intervals; (b) change in absorbance vs. irradiation time; (c) % degradation vs. irradiation time; (d) comparison of degradation rate for the decomposition of AO.

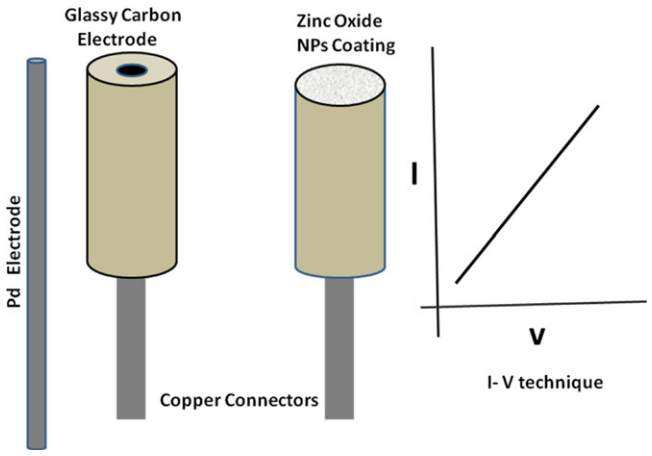

Fig. 6. Fabrication of chemical sensors using synthesized ZnO NPs and its detection methodology.

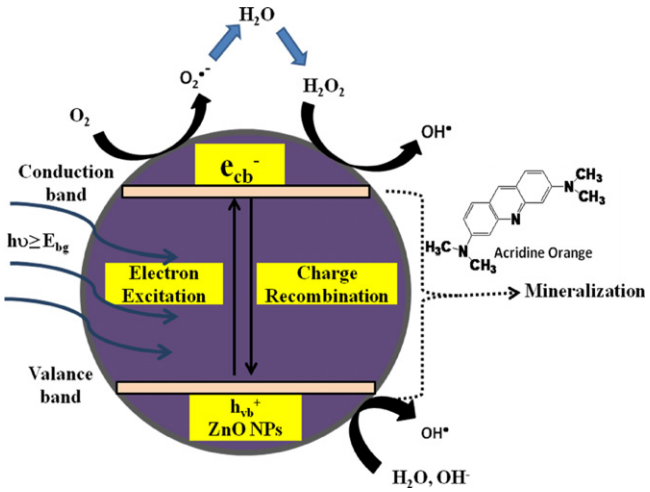

Scheme 1. Mechanism of photocatalytic degradation of AO.

degraded after 80 min of irradiation time whereas in the absence of photocatalyst no observable loss of dye could be seen. It can be seen that % degradation of AO by synthesized ZnO NPs photocatalyst after 80 min reaction time is more than commercially available TiO_2-UV100. The actual pH of solution before starting the irradiation and after 96.11% degradation of dye was 6.2 and 6.08, respectively. A slight decrease in the pH was observed at the end of experiment which may be due to the generation of proton during the course of reaction [30].

The degradation rate obtained for the decomposition of dye derivative in the presence of synthesized ZnO NPs and TiO_2-UV100 is shown in Fig. 5(d). It has been observed that degradation of dye derivative under investigation proceeds much more rapidly in the presence of synthesized ZnO NPs rather than other photocatalyst. The results above clearly indicate that the prepared NPs of ZnO photocatalyst show higher photocatalytic activity when compared with TiO_2-UV100, which might be due to its large surface area and unique structure to absorb a large fraction of UV light. Since synthesized ZnO NPs have very simple synthesis procedure, low cost and exhibited the highest overall activity for the degradation of dye under investigation, it is concluded that prepared ZnO NPs is a better photocatalyst than TiO_2-UV100 for the degradation of AO.

Earlier studies have shown that ZnO demonstrated better activity for the photocatalyitc degradation of a large number of organic pollutants. Poulios and Tsachpinis [31] showed that ZnO was found to be more effective than different semiconducting oxides viz., TiO_2 (Degussa P-25), TiO_2-UV100 and TiO_2/WO_3 when Reactive Black 5 was used as the model pollutant. Poulios et al. [32] reported that ZnO was found to be better than TiO_2 (Degussa P-25) for the degradation of Auramine O in aqueous suspension using ZnO and TiO_2 separately in batch reactor. Hoffman et al. [33] have also shown that ZnO produces H_2O_2 more efficiently than TiO_2. Thus, ZnO photo-assisted degradation may proceed in three different ways viz., photocatalytic oxidation or oxidation with photocatalytically generated H_2O_2, or simultaneous operation of both ways [20,34]. Our results for the decomposition of dye derivative under investigation are in agreement with above studies reported in the literature.

According to the mechanism of semiconductor photocatalysis, when a photon of energy equal to or greater than its band gap width irradiates ZnO nanoparticle, it leads to the formation of electron/hole (e^-/h^+) pairs with free electrons produced in the empty conduction band (e^-_{CB}) leaving behind an electron vacancy or "hole" in the valence band (h^+_{VB}). Once the charge separation is maintained the electron and hole may migrate to the surface of photocatalyst where they participate in redox reactions with organic substrate dissolved in water in the presence of oxygen. Specially, h^+_{VB} may react with surface-bound H_2O or OH^- to produce the hydroxyl radical and e^-_{CB} is picked up by oxygen to generate superoxide radical anion [35–38] as indicated in Eqs. (1)–(3) mentioned below:

$$ZnO + h\upsilon \rightarrow e^-_{CB} + h^+_{VB} \quad (1)$$

$$O_2 + e^-_{CB} \rightarrow O_2^{\bullet -} \quad (2)$$

$$H_2O + h^+_{VB} \rightarrow OH^\bullet + H^+ \quad (3)$$

Alternatively, direct absorption of light by the dye, can lead to the transfer of photogenerated electron from the excited state of the dye to the conduction band of the semiconductor which results in the generation of hydroxyl radicals and superoxide radical anions. The various steps involved in dye degradation are summarized in the following equations:

$$Dye_{ads} + h\upsilon \rightarrow Dye_{ads}* \quad (4)$$

$$Dye_{ads}* + ZnO \rightarrow Dye_{ads}{}^+ + ZnO(e^-) \quad (5)$$

$$ZnO(e^-) + O_2 \rightarrow O_2^{\bullet -} + ZnO \quad (6)$$

$$O_2^{\bullet -} + 2H_2O + e^- \rightarrow 2H_2O_2 \quad (7)$$

$$H_2O_2 + e^- \rightarrow OH^\bullet + OH^- \quad (8)$$

It has been suggested that the generated hydroxyl radicals ($OH^\bullet$) and superoxide radical anions ($O_2^{\bullet -}$) are the active oxidizers and drive the photodegradation or mineralization of the dye molecule.

Dye or Pollutant (AO) + $O_2^{\bullet -}/OH^\bullet$ → intermediates

↓

degraded or mineralized products.

Generally, the proper amount of oxygen vacancies can entrap electrons from semiconductor, resulting in the holes to diffuse to the surface of the semiconductor and causes oxidation of the organic substrate. In addition, the hydroxyl group acidity increases with decrease in electron density within the semiconductors and thus enhances the photocatalytic activity of ZnO NPs. Due to this role, increase in the number of oxygen vacancies improves the photocatalytic performance of photocatalysts.

The whole mechanism of photocatalytic degradation has been depicted in Scheme 1.

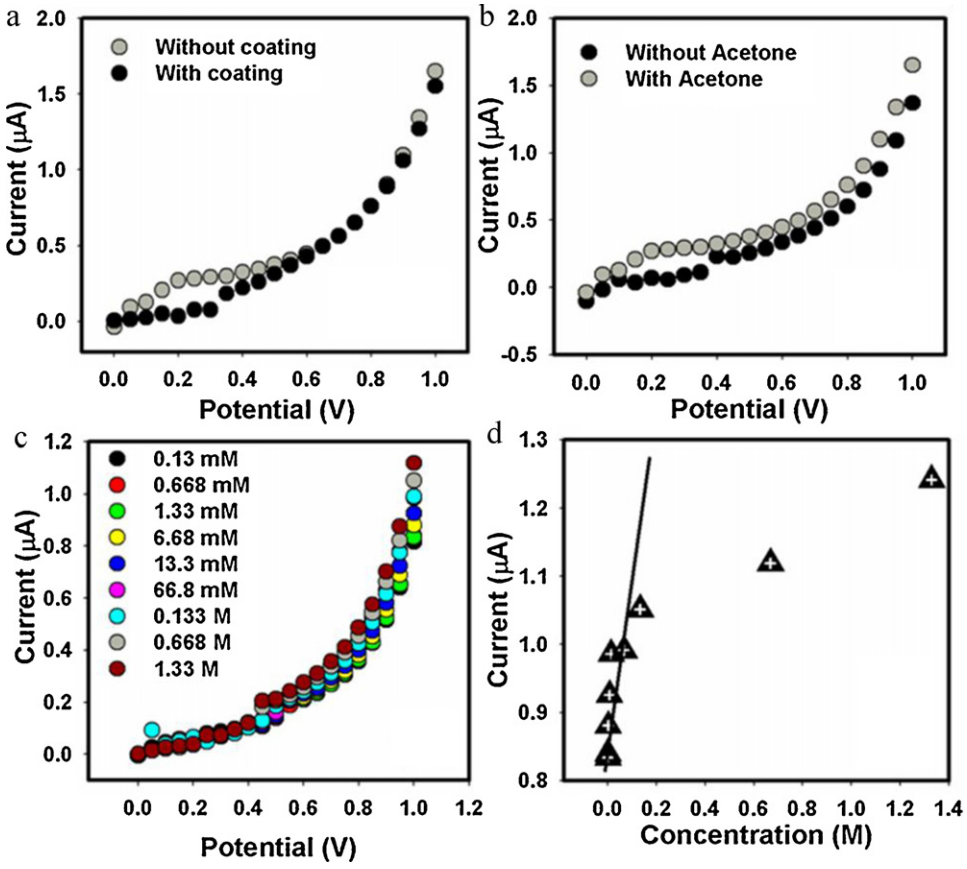

Fig. 7. *I–V* curves of (a) with and without coating of ZnO NPs; (b) with and without acetone; (c) concentration variation of acetone; and (d) calibration curve of acetone sensors.

4.2. Chemical sensing properties

The chemical sensing properties of the synthesized ZnO NPs were evaluated by detecting acetone at room temperature using *I–V* technique [7,11,12,39–42]. ZnO NPs modified electrode shown in Fig. 6 was fabricated by coating ZnO NPs on the GCE using conducting binder. Fabricated electrode was kept in oven at low temperature (60.0 °C) for 3 h until the film was completely dry and stable. The electrical response of acetone, used as a target molecule was measured using *I–V* technique.

The sensing properties of *I–V* sensors (two electrodes system) having ZnO thin film have been studied, which is presented in Fig. 6. Fig. 7(a) shows *I–V* responses of coated (with ZnO NPs) and uncoated (without ZnO NPs) electrode in which the coated electrode shows lower current as compare to the uncoated electrode which may be due to slight resistance caused by ZnO NPs with conducting binder on electrode surface. Fig. 7(b) presents the electrical response of ZnO NPs with and without acetone and exhibits an increase in the current with applied potential in the presence of acetone. The gray-solid and dark-solid dotted curves indicate the response of the film before and after injecting 100.0 μL chemicals in bulk solution. Significant increase in the sample current was observed after injection of target component. *I–V* response of ZnO NPs to varying concentration (0.13 mM to 1.33 M) of target analyte is presented in Fig. 7(c). It is observed that the current increases gradually with increase of acetone concentration. The calibration curve was plotted from the variation of acetone concentration, which is shown in Fig. 7(d). The sensitivity is calculated from the calibration curve, which was found to be 0.14065 $\mu A\,cm^{-2}\,mM^{-1}$. This sensor exhibit linear dynamic range from 0.13 mM to 0.13 M with the detection limit of 0.068 ± 0.01 mM (3 N/S). The response time was around 10 s for the NPs coated electrode to acquire saturated steady state current. The reason for elevated sensitivity of film may be due to the good absorption capability (porous surfaces fabricated with coated ZnO) and adsorption property of the zinc oxide NPs. Large surface area of ZnO NPs creates favorable nanoatmosphere for the detection of chemical and high electron communication among the active sites of NPs and GCE. These factors are responsible for the lofty sensitivity and good stability.

5. Conclusion

In summary, low-temperature growth and detailed structural and optical characterizations of well-crystalline ZnO NPs were done and demonstrated in this paper. The detailed morphological characterizations by FESEM reveal that the synthesized NPs possess almost spherical shape with the typical diameters of $\sim 50 \pm 10$ nm. The detailed structural properties examined using XRD, Raman and FTIR exhibit that the synthesized NPs are well-crystalline and possessing wurtzite hexagonal phase. The optical properties of synthesized ZnO NPs were investigated by UV–vis absorption spectroscopy which shows the presence of characteristic ZnO peak in the spectrum. For application point of view, ZnO NPs showed high photocatalytic activity when compared with commercially available TiO_2-UV100 by degrading AO. The synthesized ZnO NPs were also employed as chemi-sensor for the detection of acetone in liquid phase and explored excellent performance in terms of high sensitivity and lower detection limit. Therefore, ZnO NPs could be considered as a promising photo catalyst and chemi-sensor for environmental application.

Acknowledgements

The authors are thankful to the Deanship of Scientific Research, Najran University, Najran, Kingdom of Saudi Arabia for all financial support. Centre for Advanced Materials and Nano-Engineering (CAMNE), Najran University, Najran is highly acknowledged.

References

[1] L. Schmidt-Mende, J.L. MacManus-Driscoll, Mater. Today 10 (2007) 40.
[2] C.Q. Ge, C.S. Xie, D.W. Zeng, S.Z. Cai, J. Am. Ceram. Soc. 90 (2007) 3263.
[3] A. Umar, M.M. Rahman, S.H. Kim, Y.B. Hahn, Chem. Commun. (2008) 166.
[4] M.M. Rahman, A. Umar, K. Sawada, Sens. Actuators B 137 (2009) 327.
[5] T. Godish, Indoor Air Pollution Control, Lewis Publishers, Chelsea, MI, 1991.
[6] M. Fleischer, E. Simon, E. Rumpel, H. Ulmer, M. Harbeck, M. Wandel, C. Fietzek, U. Weimar, H. Meixner, Sens. Actuators B 83 (2002) 245.
[7] M. Faisal, S.B. Khan, M.M. Rahman, A. Jamal, A. Umar, Mater. Lett. 65 (2011) 1400.
[8] S.G. Ansari, Z.A. Ansari, R. Wahab, Y.S. Kim, G. Khang, H.S. Shin, Biosens. Bioelectron. 23 (2008) 1838.
[9] S.G Ansari, Z.A. Ansari, H.K. Seo, G.S. Kim, Y.S. Kim, G. Khang, H.S. Shin, Sens. Actuators B 132 (2008) 265.
[10] S.G. Ansari, R. Wahab, Z.A. Ansari, Y.S. Kim, G. Khang, A.A. Hajry, H.S. Shin, Sens. Actuators B 137 (2009) 566.
[11] S.B. Khan, M. Faisal, M.M. Rahman, A. Jamal, Sci. Tot. Environ. (2011), doi:10.1016/j.scitotenv.2011.04.019.
[12] M.M. Rahman, A. Jamal, S.B. Khan, M. Faisal, J. Nanoparticles Res. (2011), doi:10.1007/s11051-011-0301-7.
[13] A. Umar, Y.B. Hahn (Eds.), Metal Oxide Nanostructures and Their Applications, Part IV, American Scientific Publisher, USA, 2010.
[14] M. Faisal, M. Abu Tariq, M. Muneer, Dyes Pigments 72 (2007) 233.
[15] M. Vaseem, A. Umar, Y.B. Hahn, D.H. Kim, K.S. Lee, J.S. Jang, J.S. Lee, Catal. Commun. 10 (2008) 11.
[16] D. Ravelli, D. Dondi, M. Fagnoni, A. Albini, Chem. Soc. Rev. 38 (2009) 1999.
[17] S. Malato, P. Fernandez-Ibanez, M.I. Maldonado, J. Blanco, W. Gernjak, Catal. Today 147 (2009) 1.
[18] L.Y. Yang, S.Y. Dong, J.H. Sun, J.L. Feng, Q.H. Wu, S.P. Sun, J. Hazard. Mater. 179 (2010) 438.
[19] X.C. Song, Y.F. Zheng, E. Yang, G. Liu, Y. Zhang, H.F. Chen, Y.Y. Zhang, J. Hazard. Mater. 179 (2010) 1122.
[20] S. Anandan, A. Vinu, N. Venkatachalam, B. Arabindoo, V. Murugesan, J. Mol. Catal. A: Chem. 256 (2006) 312.
[21] J.H. Sun, S.Y. Dong, Y.K. Wang, S.P. Sun, J. Hazard. Mater. 172 (2009) 1520.
[22] R. Selvin, H.L. Hsu, N. Sabari Arul, S. Mathew, Sci. Adv. Mater. 2 (2010) 58.
[23] R.Y. Hong, J.H. Li, L.L. Chen, D.Q. Liu, H.Z. Li, Y. Zheng, J. Ding, Powder Technol. 189 (2009) 426.
[24] A. Umar, A.A. Hajry, Y.B. Hahn, D.H. Kim, Electrochim. Acta 54 (2009) 5358.
[25] A. Umar, M.M. Rahman, M. Vaseem, Y.B. Hahn, Electrochem. Commun. 11 (2009) 118.
[26] A. Umar, M.M. Rahman, A.A. Hajry, Y.B. Hahn, Talanta 78 (2009) 284.
[27] A.A. Hajry, A. Umar, Y.B. Hahn, D.H. Kim, Superlattice Microstruct. 45 (2009) 529.
[28] A. Umar, S.H. Kim, Y.S. Lee, K.S. Nahm, Y.B. Hahn, J. Cryst. Growth 282 (2005) 131.
[29] A. Umar, Y.B. Hahn, Cryst. Growth Des. 8 (2008) 2741.
[30] M.A. Rahman, M. Muneer, D. Bahnemann, Res. Chem. Intermed. 29 (2003) 35.
[31] I. Poulios, I. Tsachpinis, J. Chem. Technol. Biotechnol. 74 (1999) 349.
[32] I. Poulios, A. Avranas, E. Rekliti, A. Zouboulis, J. Chem. Technol. Biotechnol. 75 (2000) 205.
[33] M.R. Hoffman, S.T. Martin, W.Y. Choi, D.W. Bahnemann, Chem. Rev. 95 (1995) 69.
[34] E.R. Carraway, A.J. Hoffman, M.R. Hoffman, Environ. Sci. Technol. 28 (1994) 786.
[35] Y.C. Zhang, T. Qiao, X.Y. Hu, W.D. Zhou, J. Cryst. Growth 280 (2005) 652.
[36] M.Z. Tang, J.M. Wu, Sci. Adv. Mater. 1 (2009) 144.
[37] B. Pare, S.B. Jonnalagadda, H. Tomar, P. Singh, V.W. Bhagwat, Desalination 232 (2008) 80.
[38] P. Pizarro, C. Guillard, N. Perol, J.M. Herrmann, Catal. Today 101 (2005) 211.
[39] S.B. Khan, M.M. Rahman, S. Jang, K. Akhtar, H. Han, Talanta 84 (2011) 1005.
[40] M. Faisal, S.B. Khan, M.M. Rahman, A. Jamal, J. Mater. Sci. Technol., in press.
[41] M.M. Rahman, A. Jamal, S.B. Khan, M. Faisal, ACS Appl. Mater. Interface 3 (2011) 1346.
[42] M.M. Rahman, A. Jamal, S.B. Khan, M. Faisal, J. Phys. Chem. C 115 (2011) 9503.